Structural Responses to Cavity-Creating Mutations in an Integral Membrane Protein[†,‡]

Paul K. Fyfe,[§] Jane A. Potter,[||] Jade Cheng, Christopher M. Williams, Ashley J. Watson, and Michael R. Jones*

Department of Biochemistry, School of Medical Sciences, University of Bristol, University Walk, Bristol BS8 1TD, United Kingdom

Received June 4, 2007; Revised Manuscript Received July 12, 2007

ABSTRACT: X-ray crystallography has been used to investigate the extent of structural changes in mutants of the purple bacterial reaction center that assemble without a particular ubiquinone or bacteriopheophytin cofactor. In the case of the bacteriopheophytin-exclusion mutant, in which Ala M149 was replaced by Trp (AM149W), the quality of protein crystals was improved over that seen in previous work by minimizing illumination, time, and temperature during the purification protocol and carrying out crystal growth at 4 °C after overnight incubation at 18 °C. The X-ray crystal structure of the AM149W mutant, determined to a resolution of 2.2 Å, showed very little change in protein structure despite the absence of the bacteriopheophytin cofactor. Changes in the electron density map in the region of the cofactor binding site could be accounted for by changes in the conformation of the phytol side chains of adjacent cofactors and the presence of a buried water molecule. Residues lining the vacated binding pocket did not show any significant changes in conformation or increases in disorder as assessed through crystallographic atomic displacement parameters (*B*-factors). The X-ray crystal structure of a reaction center lacking the primary acceptor ubiquinone through mutation of Ala M248 to Trp (AM248W) was also determined, to a resolution of 2.8 Å. Again, despite the absence of an internal cofactor only very minor changes in protein structure were observed. This is in contrast to a previous report on a reaction center lacking this ubiquinone through mutation of Ala M260 to Trp (AM260W) where more extensive changes in structure were apparent. All three mutant reaction centers showed a decrease in thermal stability when housed in the native membrane, but this decrease was smaller for the AM260W mutant than the AM248W complex, possibly due to beneficial effects of the observed changes in protein structure. The lack of major changes in protein structure despite the absence of large internal cofactors is discussed in terms of protein rigidity, the protective influence of the adaptable membrane environment, and the role of small molecules and ions as packing material in the internal cavities created by this type of mutation.

Integral membrane proteins present a well-documented challenge to structural characterization through X-ray crystallography. The number of high-resolution X-ray crystal structures for membrane proteins increased rather slowly following early successes with proteins such as bacteriorhodopsin and the purple bacterial reaction center (RC)[1] but has undergone a significant growth during the last 5 years or so as information on how to best express and handle them has accumulated. For a small subset of membrane proteins the application of crystallography has now moved on from the initial structure characterization to investigation of detailed aspects of mechanism and protein architecture. This has mainly involved crystallization of proteins subjected to specific treatments (such as the use of inhibitors for example), crystallization of mutant complexes, or data collection under conditions designed to induce a particular state of the protein.

A small number of membrane proteins have entries in the Protein Data Bank (PDB) (*1*) for both wild-type and mutant variants. In the case of the RC some 24 of the 57 structures accessible in the PDB at the time of writing are for mutant complexes. These mutations mainly address different aspects of light-driven electron transfer (for reviews see refs *2*−*5*), including the mechanism of ubiquinone reduction and protonation (for reviews see refs *6* and *7*). In addition, a combined mutagenesis and crystallographic approach has been used to investigate lipid binding (*8*), to alter residues involved in crystal contacts (*9*), and to engineer new functionality (*10*). A summary of the structure of the RC, which in *Rhodobacter* (*Rb.*) *sphaeroides* consists of three polypeptides and ten cofactors, is shown in Figure 1. The L- and M-polypeptides form a pseudosymmetrical bundle of membrane-spanning α-helices connected by loops and

[†] This work was supported by the Biotechnology and Biological Sciences Research Council of the United Kingdom and the University of Bristol.

[‡] The structures have been deposited in the PDB under accession codes 2JIY for the AM149W RC and 2JJO for the AM248W RC.

* Corresponding author. E-mail: m.r.jones@bristol.ac.uk. Tel: 00-44-117-3312135. Fax: 00-44-117-3312168.

[§] Current address: Division of Biological Chemistry and Molecular Microbiology, Faculty of Life Sciences, University of Dundee, Nethergate, Dundee DD1 4HN, U.K.

[||] Current address: Centre for Biomolecular Sciences, University of St. Andrews, North Haugh, St. Andrews, Fife KY16 9ST, U.K.

[1] Abbreviations: BChl, bacteriochlorophyll; BPhe, bacteriopheophytin; CDL, cardiolipin; Crt, carotenoid; FTIR, Fourier transform infrared; HYD, hydrocarbon chain; LDAO, lauryldimethylamine oxide; PDB, Protein Data Bank; *Rb.*, *Rhodobacter*; RC, reaction center; Spn, spheroidenone; Ubi, ubiquinone.

10.1021/bi701085w CCC: $37.00
Published on Web 08/21/2007

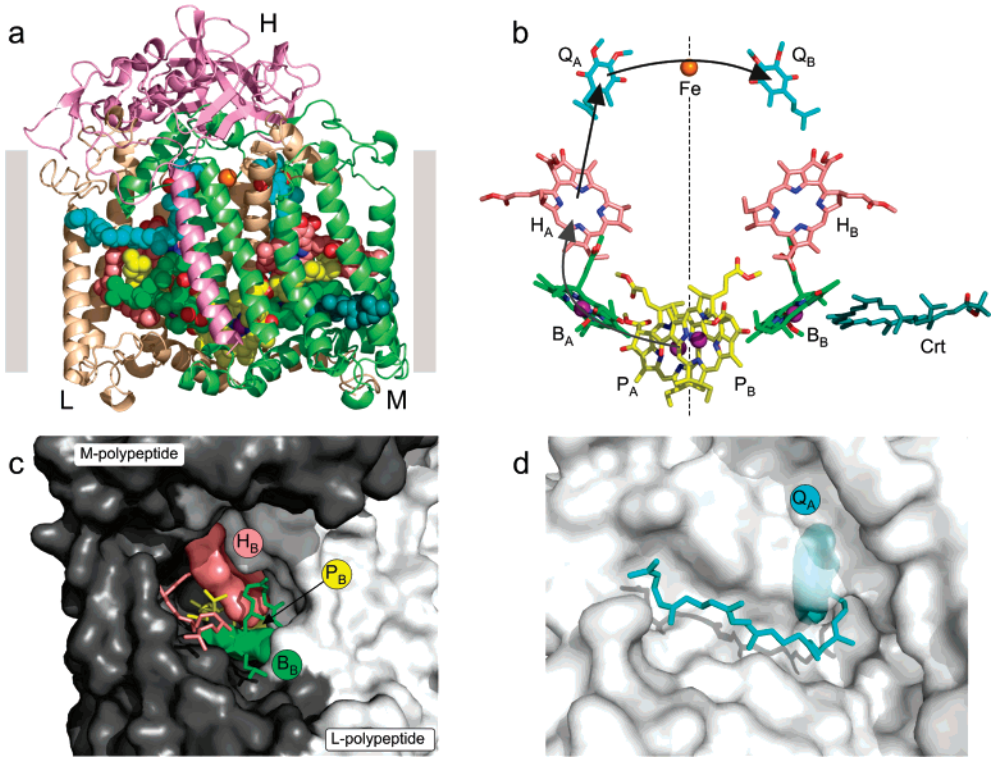

FIGURE 1: Structure and mechanism of the *Rb. sphaeroides* RC. (A) The L- (beige), M- (pale green), and H- (pink) polypeptides (ribbons) enclose ten cofactors (spheres). Gray boxes indicate the approximate position of the membrane. (b) The cofactors are arranged around an axis of 2-fold symmetry running perpendicular to the plane of the membrane (dotted line) and comprise four BChls (B_A, B_B, P_A, P_B), two BPhes (H_A, H_B), two quinones (Q_A, Q_B), a carotenoid (Crt), and an iron atom (Fe). Arrows show the route of electron transfer. (c) The BChl and BPhe cofactors are located in an extended binding cavity between the L- and M-polypeptides (white and gray surfaces). The H_B BPhe (pink), B_B BChl (green), and P_B BPhe (yellow) are partially exposed at the intramembrane surface of the protein; bacteriochlorin macrocycles are shown as solid objects and phytol side chains as sticks. (d) The headgroup of the Q_A ubiquinone (cyan spheres) is embedded in the M-polypeptide (white solid object, made semitransparent near the Q_A pocket), with the isoprenoid side chain emerging into the membrane interior.

short helices on either side of the membrane (Figure 1a), and this protein scaffold encases four bacteriochlorophylls (BChl), two bacteriopheophytins (BPhe), two ubiquinones, a carotenoid, and an iron atom (Figure 1b). The BChl, BPhe, and ubiquinone cofactors are arranged in two pseudosymmetrical membrane-spanning branches, one of which is used to catalyze photochemical charge separation (see refs *3*, *4*, and *11*−*13* for reviews on structure and mechanism). Of particular note for the present report are the characters of the binding sites of the Q_A ubiquinone and the H_B BPhe and B_B BChl. The bacteriochlorin cofactors occupy a deep cleft between the L- and M-polypeptides that is exposed to the membrane interior. Figure 1c shows a view in the plane of the membrane of part of this cavity, with the bacteriochlorin macrocycles and surrounding protein rendered as solid objects and the phytol chains of the bacteriochlorins as sticks. The macrocycle of the P_B BChl is just visible, underlying those of the B_B BChl and H_B BPhe, and all of the bacteriochlorins are sandwiched between the M- and L-polypeptides. As shown in Figure 1d, the headgroup of the Q_A ubiquinone occupies a cavity internal to the M-polypeptide (the protein is shown as a white solid object, made semitransparent near the Q_A pocket). The resolved part of the isoprenoid side chain emerges from the protein interior and packs in a groove in the intramembrane surface.

The majority of X-ray crystal structures for mutant RCs deposited in the PDB show very limited changes from the wild-type structure, reflecting the use of mutagenesis to affect a particular aspect of RC function in a highly specific way. However, a small subset of deposited structures show more extensive structural changes, either because the mutation introduced unintended (and usually unwanted) longer range changes in structure or in one case because the mutation was designed to cause the RC to assemble without a key cofactor (*14*). In mutants of the latter type, high-resolution structural information provides an opportunity to examine how different parts of the protein respond to the absence of a major cofactor and to attempt to relate structural changes to changes in the stability of the protein.

Structural information on two such cofactor-exclusion mutants has been published. In 2000, McAuley and co-workers described a 2.1 Å resolution crystal structure of a RC with an Ala to Trp mutation at position 260 of the M-polypeptide (denoted AM260W; PDB entry 1QOV) (*14*). This Ala residue forms part of the binding pocket of the redox-active headgroup of the Q_A ubiquinone, and mutation of this residue to a bulky Trp caused the RC to assemble without this ubiquinone (*15*−*17*). This change in structure was accompanied by some changes in the conformation of a loop of four amino acids (M256−M259) immediately adjacent to the M260 position (*14*). More recently, Watson and co-workers reported a low-resolution X-ray crystal structure of a RC with an Ala to Trp mutation at residue 149 of the M-polypeptide (denoted AM149W) (*18*). Although the quality and resolution of the diffraction data were limited and the structure was only partially refined, the electron density maps were consistent with a conclusion drawn from absorbance and Fourier transform infrared

(FTIR) spectroscopy that the AM149W RC assembles without the BPhe cofactor at the H_B position. The resulting surface-exposed void contained a number of electron density features that could not be assigned due to the limited quality of the electron density maps.

In the present report a greatly improved structure for the AM149W RC is described, at a resolution of 2.2 Å, together with the structure of a RC with a mutation of Ala M248 to Trp (AM248W) that also assembles without a Q_A ubiquinone (*15*). The extents of the protein structural changes that result from exclusion of these large cofactors are discussed, including the rigidity of the protein that forms the binding pocket and the incorporation of foreign molecules as "packing material" to fill the void spaces created and satisfy potentially destabilizing bonding interactions. The effects of these mutations on the stability of the membrane-bound RC are also examined and discussed in the light of the observed changes in structure.

EXPERIMENTAL PROCEDURES

Reaction Center Mutagenesis, Purification, and Crystallization. Construction of the AM260W, AM248W, and AM149W mutations has been described previously (*15*, *18*). For the purification of the AM248W and AM149W RCs, intracytoplasmic membrane fragments were prepared from cells of antenna-deficient strains that had been grown under semiaerobic conditions in the dark, using procedures described previously (*19*). RCs were solubilized from membrane fragments suspended in 20 mM Tris-HCl (pH 8.0) by the addition of NaCl to 100 mM followed by lauryldimethylamine oxide (LDAO) to 0.3%. Solubilized RCs were purified by two sequential passes through a DE52 anion-exchange column (Whatman), followed by passage through a Sepharose Q and Sephadex 200 column (Pharmacia), as described in detail elsewhere (*19*). For the AM149W RC, which had shown a tendency to be unstable in previous studies (*18*), all chromatographic steps were performed under low light conditions using buffers that had been precooled on ice.

Trigonal crystals, space group $P3_121$, were grown by sitting drop vapor diffusion as described previously (*19*) (and see text). Well solutions containing 9 mg mL^{-1} RC, 0.09% (v/v) LDAO, 3.5% (w/v) heptane-1,2,3-triol, and 0.7 M potassium phosphate (pH 8.0) were equilibrated against a reservoir solution of 1.4 M potassium phosphate in incubations carried out at 18 °C. For the AM149W RC a duplicate set of trays was generated and incubated at 4 °C for 2 weeks, followed by overnight incubation at 18 °C and then further incubation at 4 °C (see text). Crystals grown at 18 °C appeared within 1−2 weeks, while those incubated at 4 °C presented useful crystals by the end of the third week.

Data Collection and Refinement. X-ray diffraction data were collected at 100 K using cryocooled crystals and an ADSC Quantum 4 detector on beamline 14.1 of the Daresbury Synchrotron Facility, U.K. Crystals were prepared for cryocooling by sequential soaking in mother liquor containing increasing concentrations of ethylene glycol to give a final concentration of 25%. Data for the AM149W RC were collected from a single cryocooled crystal over the range 16−2.2 Å; the crystal had unit cell dimensions of $a = b =$ 139.8 Å, $c = 185.45$ Å, $\alpha = \beta = 90°$, and $\gamma = 120°$. Data for the AM248W RC were collected from 28 to 2.8 Å, and the crystals had unit cell dimensions $a = b =$139.81 Å and $c = 185.15$ Å.

Table 1: Crystallographic Statistics for Data Collection and Refinement

	AM149W	AM248W
PDB entry	2JIY	2JJO
data collection		
resolution range (Å)	15.97−2.20	27.9−2.8
outer shell (Å)	2.26−2.20	2.87−2.8
unique reflections	104522	51507
R_{merge} (%)[a,b]	6.4 (49.9)	7.5 (52.6)
completeness (%)[a]	98.5 (98.2)	98.9 (99.4)
redundancy[a]	3.8 (3.8)	2.0 (2.0)
Wilson *B*	34.8	37.2
refinement		
resolution (Å)	15.97−2.20	27.9−2.8
reflections	99574	48879
R_{cryst} (%)[c]	18.2	20.3
R_{free} (%)[d]	20.7	24.5
rmsd, bond (Å)	0.01	0.013
rmsd, bond angle (deg)	1.373	1.462
coordinate error (Å)[e]	0.14	0.34
model		
no. of protein residues[f]	822	817
no. of cofactors[g]	4 BChl, 1 BPhe, 2 Ubi, 1 Fe, 1 Spn	4 BChl, 2 BPhe, 1 Ubi, 1 Fe, 1 Spn
no. of waters	363	122
other components[g]	2 LDAO, 2 HYD, 1 CDL, 1 phosphate	1 CDL, 1 chloride

[a] Values in parentheses are for the outer resolution shell. [b] $R_{merge} = \sum_h\sum_i|\langle I(h)\rangle - I(h)_i|/\sum_h\sum_i I(h)_i$, where $I(h)$ is the intensity of reflection h, $\sum_h$ is the sum over all reflections, and $\sum_i$ is the sum over all i measurements of reflection h. [c] R_{cryst} is defined by $\sum||F_o| - |F_c||/\sum|F_o|$. [d] R_{free} was calculated with 5% reflections selected to be the same as in the refinement of the wild-type reaction center (*19*). [e] Coordinate error was estimated by Cruickshank's DPI (*34*). [f] Models differ by five amino acids at the C-terminus of the H-polypeptide that were not included in the lower resolution structure. [g] Abbreviations: Ubi, ubiquinone; Spn, spheroidenone (carotenoid); HYD, hydrocarbon chain; CDL, cardiolipin.

The two data sets were processed and scaled using HKL2000 (*20*), and molecular replacement was performed using AMORE (*21*) using the coordinates of the wild-type RC as the search model. Refinement was performed using restrained maximum likelihood refinement in REFMAC 5.0 (*22*). The collection and refinement statistics are given in Table 1, and the structures have been deposited in the PDB under accession codes 2JIY for the AM149W RC and 2JJO for the AM248W RC. The structure of the AM260W RC determined in previous work (*14*) is available in the PDB under accession code 1QOV.

Thermal Stability. To assess the thermal stability of the membrane-embedded RC, antenna-deficient intracytoplasmic membranes were diluted to a RC concentration of 0.1 mM in 20 mM Tris-HCl (pH 8.0) and split into eleven 1 mL aliquots. Ten of these were incubated in a water bath at 70 °C, and the eleventh was placed on ice to act as a reference sample. Aliquots were removed at defined time intervals and rapidly cooled to 4 °C on ice. Absorbance spectra were recorded between 400 and 1000 nm following the addition of 1 mM sodium ascorbate and 25 μM phenazine methosulfate to ensure full reduction of the P BChls. All absorbance spectra were corrected for background scatter between 650 and 950 nm, and the data were analyzed by

plotting the absorbance at 804 nm after incubation of membranes for a given time as a fraction of the absorbance at 804 nm in the reference spectrum of unheated membranes. The data shown are the average of at least three experiments.

RESULTS

Crystallization of the AM149W RC. Spectroscopic studies have established that mutagenesis of Ala M149 to Trp causes the RC to assemble in the membrane without the BPhe at the H_B position (*18*). A previous partially refined X-ray crystal structure for the AM149W RC, based on diffraction data collected to a resolution of 3.4 Å, supported this conclusion (*18*). The resolution of the data obtained for crystals of the AM149W RC in that study was atypically low, and it was noted that this particular mutant complex showed a tendency to degrade during column purification (which is carried out at room temperature), with the appearance of free BChl in column eluates. Thus although a sufficient quantity of pure AM149W RC was obtained for crystallization, this tendency to degrade led to relatively poor quality crystals, possibly due to RCs undergoing further degradation during incubation of crystal trays.

In the present study a number of modifications were made to the standard purification and crystallization procedure. Problems signified by the appearance of free BChl in column eluates were overcome by carrying out all chromatography procedures under low light conditions, precooling all buffers to 4 °C, and minimizing delays between consecutive chromatography steps. These adaptations enabled the purification of sufficient quantities of the AM149W complex for crystallization with minimal losses due to degradation.

Trigonal crystals of the AM149W RC were grown by sitting drop vapor diffusion as described previously (*19*). In addition to the normal incubation of crystal trays at 18 °C a duplicate set of trays was generated and incubated at 4 °C to determine whether crystals of a potentially unstable mutant could be grown at this temperature. Crystals grown at 18 °C appeared within 1−2 weeks, which is typical for the crystallization of the RC by this method. The trays incubated at 4 °C showed only very limited crystal growth after 2 weeks, although the presence of a couple of sizable crystals suggested that a reduced rate of nucleation rather than crystal growth was preventing the appearance of larger numbers of crystals. The trays were therefore moved to 18 °C overnight in an attempt to encourage nucleation and then returned to 4 °C for subsequent growth to continue at a low temperature. Significant numbers of useful crystals appeared approximately 1 week after this "heat shock", suggesting that nucleation was indeed a limiting factor at 4 °C. Regardless of the incubation temperature crystals of the AM149W RC had identical (and expected) morphologies, presenting as prisms of hexagonal cross section and variable size.

X-ray Crystal Structure of the AM149W RC. The X-ray crystal structure of the AM149W RC was determined as described in Experimental Procedures. Data were collected from a single cryocooled crystal taken from a tray that had been incubated at 4 °C. Diffraction occurred up to a higher resolution limit of 2.2 Å, and the data showed excellent redundancy and completeness (see Table 1 for statistics on data collection and refinement). The resolution and quality of these data were a significant improvement on the 3.4 Å dataset described previously, indicating that the changes to the purification and crystallization procedures outlined above had produced higher quality crystals. As expected, the final fully refined structure based on the 2.2 Å data set had much lower *R*-factors (R_{cryst} = 18.1%, R_{free} = 20.7%; Table 1) than the partially refined structure based on the 3.4 Å dataset [R_{cryst} = 24.5%, R_{free} = 29% (*18*)]. With the exception of the changes discussed below that are localized to the binding pocket of the H_B cofactor, the structure of the AM149W RC showed no significant differences to that of the wild-type RC.

On comparison with data for the wild-type complex, significant changes were observed in the electron density map for the AM149W RC in the region of the H_B cofactor. The principal changes were consistent with those observed in the previous study (*18*), but the much improved quality of the density allowed modeling to be carried out with more confidence. Electron density corresponding to the H_B cofactor was absent in the data for the AM149W RC, and clear density was observed for the new Trp residue at the M149 position. Immediately adjacent to the nitrogen of the Trp side chain was a spherical electron density feature that was consistent with a water molecule and was modeled as such. This water is located roughly at the center of the membrane, in the deepest part of the cavity created by the absence of the H_B macrocycle.

No significant changes were observed in the orientations of the amino acid residues lining the binding pocket (see below), but changes were seen in the orientation of the phytol chains of the P_B and B_B cofactors, both of which form part of the environment of the H_B cofactor in the wild-type RC. Figure 2a shows a superposition of selected elements from the structural models of the AM149W and wild-type RCs to illustrate these changes. In the wild-type RC residue Ala M149 forms part of the membrane-spanning C helix of the M-polypeptide (shown as a tube in Figure 2a, with the side chain methyl indicated by an arrow). The Trp at this position in the AM149W RC was oriented approximately coplanar with the BPhe macrocycle in the wild-type RC and occupied space normally taken up by atoms of ring III of the macrocycle and rings II and V to a lesser extent. The presence of this Trp therefore precluded binding of the BPhe in its normal position. The new water located adjacent to the indole nitrogen of Trp M149 is shown as a large sphere in Figure 2a.

The low-resolution structural data described previously also included an unattributed electron density feature overlapping with the expected position of ring V of the BPhe macrocycle (labeled A in ref *18*). In the new data this density feature could be attributed to the phytol side chain one of the primary donor BChls (P_B). In the wild-type RC the phytol chain of P_B packs against the macrocycle of H_B and emerges from the body of the protein between the phytol chains of H_B and B_B; this conformation of the P_B chain is labeled as "normal" in Figure 2a. In the AM149W mutant the phytol chain of P_B appeared to have changed its position for approximately half its length to occupy part of the void created following exclusion of H_B (labeled "alternative" in Figure 2a with carbon atoms in the new conformation highlighted in ball-and-stick format). Analysis of the electron density map suggested that the altered conformation had occurred in 65% of the complexes in the crystal, with the

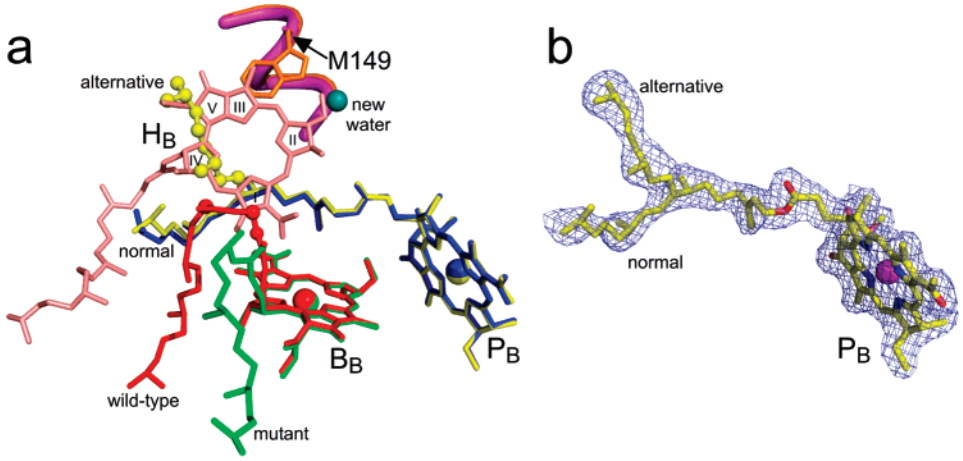

FIGURE 2: Structure of the AM149W RC. (A) Overlay of the structures of the wild-type and AM149W RCs. The M149 amino acid forms part of the membrane-spanning C helix of the M-polypeptide (magenta and orange tubes and sticks in wild type and AM149W, respectively). The H_B BPhe (pink sticks) is absent in the AM149W RC. The phytol chain of the P_B BChl (blue or yellow sticks in wild type and AM149W RC, respectively) partially occupies an alternative conformation in the AM149W RC (yellow ball-and-stick representation). A water molecule is also found in the deepest part of the cavity created in the AM149W RC (teal sphere). Part of the phytol chain of the B_B BChl in the wild-type RC (red sticks) is in van der Waals contact with the H_B BPhe (atoms indicated by red ball-and-stick representation). In the AM149W RC the conformation of the phytol chain of B_B is altered (green sticks). (b) Fit of the structural model of the P_B BChl to the corresponding electron density, showing branching of the phytol side chain in the AM149W RC.

remaining 35% having the normal conformation (stick model). These percentages, which are only approximate values, were derived through rounds of model building with subsequent investigation of the electron density maps and the atomic displacement parameters (*B*-factors). In the alternative conformation the phytol chain of P_B took up space normally occupied by rings IV and V of the macrocycle of H_B. The two conformations of the phytol chain of the P_B BChl in the AM149W RC are also presented in Figure 2b, which shows the fit of the structural model to the electron density; the branching in the electron density is clearly visible, and both branches of electron density were continuous to the end of the phytol chain.

The second significant change in structure was a repacking of the phytol chain of the B_B BChl, the native conformation of which is shown in red in Figure 2a (labeled "wild-type"). In the wild-type RC some of the atoms of this chain, highlighted as small red spheres in Figure 2a, are in van der Waals contact with atoms of ring I of the H_B cofactor. In the mutant complex the chain of B_B packed further away from the usual position of the H_B cofactor, possibly as a result of a destabilization caused by loss of these van der Waals interactions (labeled "mutant" in Figure 2a).

The center of the cavity created by the absence of the BPhe was occupied by two "blobs" of electron density that were not connected to the density of the surrounding protein (not shown). The sizes of these features were consistent with several connected atoms, but their shapes were insufficiently distinct to permit modeling. Further electron density features of uncertain origin were seen near the mouth of the cavity, at the protein surface, and these were similar to other blobs and tubes of density that are routinely observed over all parts of the protein surface. There are several candidates in the crystallization mix that could account for such features, such as the detergent LDAO, the small amphiphile heptane-1,2,3-triol, and lipids that have remained associated with the RC during purification.

Given the relatively large size of the H_B cofactor, perhaps the most surprising aspect of the structure of the AM149W RC was a lack of any significant changes in the conformation of the 17 or so amino acids that form the binding pocket. This is illustrated in the stereoviews in Figure 3, which compare the cavity between the L- and M-polypeptides that accommodates the H_B and B_B macrocycles in the wild-type and AM149W RC, respectively. In these representations the protein is shown as a solid object, the cofactors are shown as stick models (color coding as in Figure 2a), and the view is approximately in the plane of the membrane. In the wild-type RC Ala M149 (magenta surface in the center view in Figure 3a) is adjacent to the most deeply buried part of the H_B macrocycle. In the AM149W RC the bulkier Trp M149 (orange surface in the center view in Figure 3b) occludes the most deeply buried part of the H_B binding cavity, as does the adjacent water molecule (sphere). The H_B cofactor is absent, and the alternative conformation of the phytol chain of P_B (ball-and-stick format) can be seen extending upward into the vacated space. In the wild-type complex the phytol chain of B_B packs against the macrocycle of H_B and the bottom of the cofactor-binding cavity (Figure 3a), whereas in the mutant complex this chain packs against the right-hand side of the cavity (Figure 3b).

Comparison of the contours of the protein surface in Figure 3 highlights the fact that the absence of the H_B cofactor and repacking of the phytol chain of B_B in the AM149W RC caused very little disturbance to the encasing protein scaffold, which is made up from side chains and backbone atoms from a number of membrane-spanning α-helices. Furthermore, it was apparent from an analysis of crystallographic *B*-factors that the residues lining the H_B pocket were not significantly more disordered as a result of the absence of the H_B cofactor. In the AM149W structural model the average *B*-factor of all atoms located within 6 Å of the usual position of the H_B cofactor had a value of 44.7, compared with 42.9 for all of the atoms in the AM149W model. In the (lower resolution) structure of the wild-type RC the equivalent average *B*-factors had values of 59.3 and 60.9.

A final point to note is that the stereoviews in Figure 3 also show the position of the Q_B ubiquinone, the cofactor

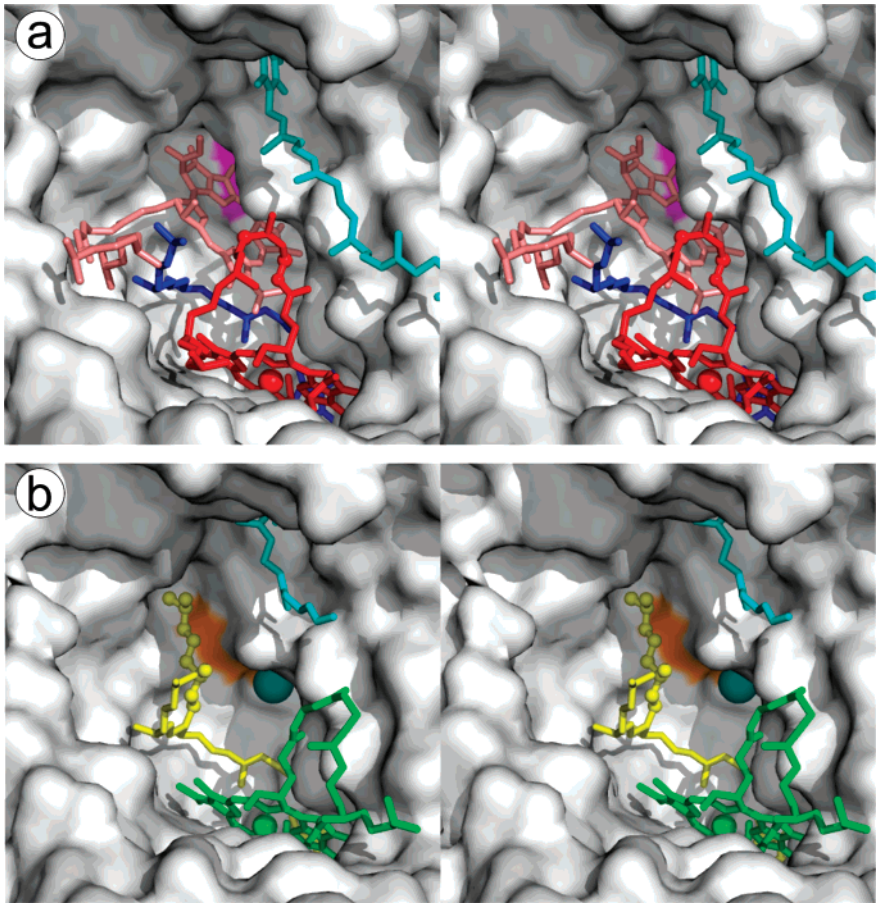

FIGURE 3: Stereoview of the binding cleft of the H_B, B_B, and P_B cofactors. The protein is shown as a solid object, cofactors are shown as sticks, and the view is approximately in the plane of the membrane. (a) Wild-type RC showing Ala M149 as a magenta surface and the remainder of the protein in gray. Cofactors are H_B (pink), B_B (red), P_B (blue), and Q_B (cyan). (b) AM149W RC showing Trp M149 as an orange surface and the remainder of the protein in gray. Cofactors are B_B (green), P_B (yellow), and Q_B (cyan). The new water adjacent to Trp M149 is shown as a teal sphere.

that detaches from the RC in order to deliver electrons to the cytochrome bc_1 complex. In this particular model of the wild-type RC the headgroup of the Q_B quinone occupies the so-called "distal" binding position and so is partially visible in the view shown in Figure 3a. Most of the isoprenoid chain of the quinone is included in the structural model and extends along the protein surface toward the center of the membrane. In the structure of the AM149W mutant the quinone headgroup occupied the more deeply inserted "proximal" binding position and only part of the isoprenoid chain could be traced (Figure 3b). However, there was no indication that these differences were a consequence of the AM149W mutation, as the modeled conformation of this particular cofactor shows a great deal of variety in the RC structures deposited in the PDB, reflecting its mobile character.

X-ray Crystal Structure of the AM248W RC. Spectroscopic studies have established that mutagenesis of Ala M260 or Ala M248 to Trp causes the RC to assemble without the Q_A ubiquinone (*15*). The X-ray crystal structure of the AM260W mutant was reported in a previous study (*14*), and in the present work the X-ray crystal structure of the AM248W complex was determined on the basis of diffraction data recorded over the range 28.0−2.8 Å (see Table 1 for statistics on data collection and refinement).

In the maps calculated for the AM248W RC the electron density feature usually attributed to the Q_A ubiquinone was completely absent, as expected. A new density feature deep in the Q_A binding pocket could be modeled as the side chain of a Trp residue at the M248 position. Figure 4a shows details from an overlay of the structures of the wild-type and AM248W RC. This figure shows the cytoplasmic halves of the so-called D and E membrane-spanning α-helices of the M-polypeptide that are connected by two loops and a shorter α-helix, termed de, that runs at approximately 45° to the plane of the membrane. The backbone of the M-polypeptide in the wild-type and AM248W RC is shown in green and yellow, respectively, as are the carbon atoms of selected amino acid residues (oxygen and nitrogen shown in red and blue, respectively). The inset to Figure 4a shows an enlarged and slightly rotated view of the M248 residue and the headgroup of the Q_A ubiquinone (sticks with cyan carbons). The CB carbon of the new Trp side chain was located in approximately the position usually occupied by the CB carbon of the wild-type Ala M248, and the remainder of the side chain projected into the Q_A binding pocket. The Trp side chain in the AM248W RC overlapped with several atoms of the Q_A headgroup in the wild-type RC, and these are indicated by small cyan or red spheres in the inset to Figure 4a. Thus it would appear that the Q_A ubiquinone was not assembled into the AM248W RC due to occlusion of a significant portion of the binding pocket of the headgroup.

A similar result was obtained in previous work for the AM260W RC, and equivalent views of an overlay of the structures of the WT and AM260W RCs are shown in Figure

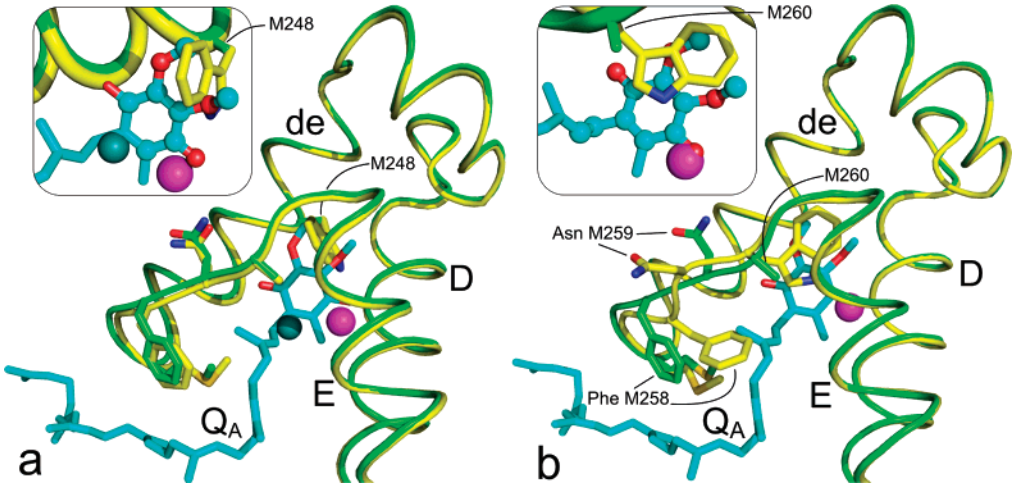

FIGURE 4: Changes in the structures of the Q_A-deficient RCs. (a) Overlay of the backbone fold of the M-polypeptide in the wild-type (green) and AM248W (yellow) RC. Residues M248 and M256−260 are shown in sticks with green and yellow carbons, respectively, for the wild-type and mutant RC, with oxygens in red and nitrogens in blue. In the mutant RC a chloride (magenta sphere) and water (teal sphere) occupy space occupied by the headgroup of the Q_A ubiquinone in the wild-type RC (sticks with cyan carbons). The inset shows an enlarged and rotated view of Trp M248 and the Q_A headgroup. Atoms in the latter that overlap with Trp M248 are shown in ball-and-stick representation. (b) Equivalent representation of an overlay of the structures of the wild-type and AM260W RC, showing shifts in the positions of amino acids M257−M260.

4b. As can be seen in the inset to Figure 4b, the new Trp side chain at the M260 position projects into the Q_A binding pocket and occupies space normally occupied by most of the atoms of the Q_A headgroup.

The AM248W mutation did not bring about any major changes in the structure of the amino acid residues lining the Q_A pocket or the fold of the polypeptide backbone. This is evident in Figure 4a, which shows the polypeptide backbone of the WT and AM248W RC. A few residues showed very small shifts in position, but all of these involved maximal displacements of equivalent atoms of less than 1 Å, and so it could be concluded that the structure of the pocket was well conserved, with no collapse of amino acid side chains into the internal cavity created by exclusion of Q_A. This is in contrast to previous data obtained with the AM260W RC (Figure 4b), as considered in more detail in the Discussion.

Two spherical electron density features were seen in the data for the AM248W RC at positions normally occupied by the Q_A headgroup in the wild-type complex. The first of these, located close to the usual position of C6 of the Q_A ring, was consistent with a water molecule and was modeled as such (Figure 4a). The second was an intense feature that had similar characteristics to a spherical electron density feature described in the previous report on the AM260W mutant RC and attributed in that study to a chloride ion (*14*). An equivalent view of an overlay of the structures of the wild-type and AM260W RCs is shown in Figure 4b, with the chloride shown as a magenta sphere. This chloride has also been included in the X-ray structure of a RC with five mutations, including AM260W, reported by Paddock and co-workers (*23*). Following the same arguments as those presented previously (*14*), the intense feature in the electron density map of the AM248W RC was also attributed to a chloride ion (Figure 4a). It showed a number of potential bonding interactions, being located approximately 3.3 Å from the indole nitrogen of Trp M248, 3.3 Å from the ND nitrogen of His M219, 3.1 Å from the new modeled water molecule, and 3.8 Å from the indole nitrogen of Trp M252. The remainder of the Q_A pocket and short channel leading to the intramembrane surface of the protein contained fragmented electron density that could not be modeled.

Thermal Stability of Membrane-Bound Mutant RCs. The effects of the cofactor-excluding mutations on the thermal stability of the membrane-bound RC were assessed by monitoring the absorbance spectrum of the bacteriochlorin cofactors, as described in detail recently (*24*, *25*). The so-called Q_y absorbance bands of these cofactors are significantly red shifted compared to those of the corresponding free bacteriochlorins and so can be used as convenient and sensitive indicators of the structural integrity of the RC. Figure 5a shows the near-infrared absorbance spectrum of antenna-deficient membranes containing wild-type RCs. This figure compares the spectrum of membranes that had not been heated with spectra recorded after incubation for 5, 10, or 100 min at 70 °C followed by rapid cooling to 4 °C. The spectrum of unheated membranes consists of three principal absorbance bands. The band at 756 nm is attributable to the Q_y transitions of the two RC BPhes. The band at 867 nm is attributable to the low-energy exciton component of the Q_y transition of the primary donor (P) BChls; as shown in Figure 1b these form an excitonically coupled dimer at the periplasmic end of the complex. The band at 804 nm is attributable to the Q_y transitions of the two so-called monomeric BChls, together with a contribution from the high-energy exciton component of the Q_y transition of the P BChls. Following heating at 70 °C, dissociation of the complex is indicated by strong decreases in absorbance at 867 and 804 nm (Figure 5a). The changes are accompanied by an increase in absorbance around 680 nm due to the appearance of free BChl and BPhe. The absorbance changes in the 760 nm region are complex, as discussed in detail in a recent report (*25*), involving loss of the native BPhe absorbance and the appearance of absorbance due to free BChl and BPhe. Loss of structural integrity of the RC can be monitored by following the absorbance decreases at 804 or 867 nm as function of time or temperature.

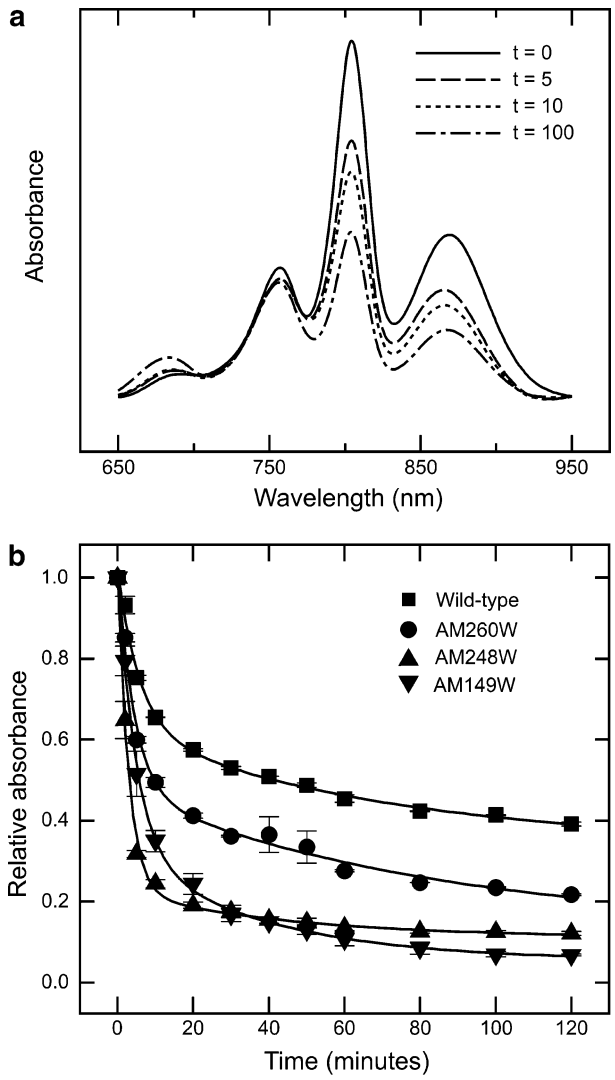

FIGURE 5: Thermal stability of membrane-bound RCs. (a) Changes in the absorbance spectrum of membrane-bound wild-type RCs on heating at 70 °C for various times. Spectra have been corrected for background scatter between 650 and 950 nm. (b) Absorbance of membrane-embedded RCs at 804 nm after various periods of heating at 70 °C relative to absorbance at 804 nm in an unheated sample. The results of biexponential fits are shown with time constants (and amplitudes): wild type, $\tau_1 = 5.8$ s ($a_1 = 0.39$), $\tau_2 = 72$ s ($a_2 = 0.29$); AM260W, $\tau_1 = 4.5$ s ($a_1 = 0.54$), $\tau_2 = 83$ s ($a_2 = 0.35$); AM248W, $\tau_1 = 2.9$ s ($a_1 = 0.78$), $\tau_2 = 45$ s ($a_2 = 0.12$); AM149W, $\tau_1 = 4.8$ s ($a_1 = 0.67$), $\tau_2 = 37$ s ($a_2 = 0.30$).

Figure 5b shows the response of antenna-deficient membranes containing wild-type RCs to incubation at 70 °C, measured by plotting the intensity of the 804 nm absorbance band as a fraction of the intensity of the same band in a spectrum of unheated membranes. The data could be fitted as a two-exponential decay with time constants of 5.9 and 72 min. This biexponential decay was in qualitative agreement with data reported recently for wild-type RCs in liposomes, which also showed a biexponential decay of absorbance at 800 nm on heating (*25*). Also in agreement with previous data it was found that the kinetics of decay of the P Q_y band were coincident with those of the B Q_y band (not shown).

Figure 5b also shows equivalent data for the AM260W, AM248W, and AM149W cofactor-exclusion mutants. All three mutant complexes showed a decrease in stability compared to the wild-type complex, with the fast and slow phases of the decay being affected differently in the three mutants in terms of rate and amplitude (see legend to Figure 5). All three mutants showed an acceleration of the fast phase, with varying effects on the slower phase. The AM260W mutant was the least affected overall, with the remaining mutants showing similar overall decreases in stability over the period of the experiment. These data were highly reproducible, the same trends being seen in experiments performed on different membrane preparations.

DISCUSSION

As discussed elsewhere (*5*, *14*, *15*, *18*), the cofactor-excluding mutations described in this and previous reports provide useful ways of modulating the electron-transfer properties of the RC and unmasking the spectroscopic properties of remaining cofactors. An essential element of the use of these mutations as experimental tools is a proper understanding of their structural consequences, as BPhe and ubiquinone are large molecules that occupy extensive intraprotein binding pockets. One of the purposes of the work described in the present report was therefore to describe X-ray crystal structures for the AM149W and AM248W complexes, to go alongside structural data on the AM260W RC that was reported some years ago (*14*). However, in a more general context these structures also provide an opportunity to look at how a multicomponent membrane protein responds to the absence of a major structural element such as a large cofactor. Information on the structure of membrane proteins is limited, and the mutant complexes that have been structurally characterized tend to have small changes in structure, targeted to a particular residue or residue−cofactor interaction. High-resolution crystallographic information on mutant membrane proteins with larger scale changes in composition is very rare.

Exclusion of Large Cofactors Produces Very Limited Changes in Protein Structure. Perhaps the most striking aspect of the structures described in the present report was the lack of any significant rearrangement of the residues that form the environments of the H_B BPhe or Q_A ubiquinone. In the case of H_B the binding cleft is lined by the residues of around 17 amino acids, together with atoms from the P_B BChl, B_B BChl, and Q_B ubiquinone. The conformations of these amino acid residues and the polypeptide backbone were largely unaffected by the absence of the H_B cofactor, over and above minor variations expected when comparing two structures determined at resolutions of between 2 and 3 Å. The exceptions to this were Phe L216, Val L220, and Leu L185, which showed some very small shifts in conformation. In addition, the residues lining the binding cleft did not exhibit increases in disorder following exclusion of the BPhe, as assessed from their crystallographic *B*-factors. Of course, the cavity resulting from the absence of H_B is unlikely to be empty in the crystallized RC, with disordered solvent probably filling those parts not occupied by the alternative conformation of the phytol chain of P_B (see Figures 2 and 3b). A similar lack of significant rearrangement was also seen for the Q_A pocket in the AM248W RC. Again, this points to a rather rigid protein structure, where the absence of a major cofactor can be tolerated without significant changes to the surrounding protein.

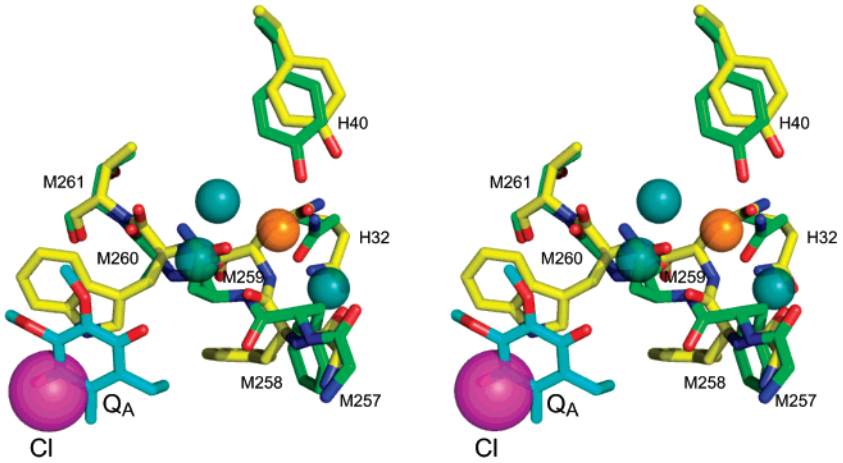

FIGURE 6: Changes in the structure of the AM260W RC. Stereoview of an overlay of amino acids M257−261 in the wild-type and AM260W RCs (green and yellow carbons, respectively) plus the side chains of amino acids Tyr H40 and Gln H32. In the mutant RC a chloride (magenta sphere) occupies space occupied by the headgroup of the Q_A ubiquinone (sticks, cyan carbons) in the wild-type RC. In the AM260W RC repositioning of the side chain of Asn M259 causes the exclusion of a water molecule found in the wild-type RC (orange sphere) and creates a space that is occupied by two new water molecules in the AM260W RC (teal spheres in the center view). A third water in the AM260W RC (teal sphere on the right) occupies space created by repositioning of the side chain of Phe M258.

The results obtained with the AM248W RC were rather different compared to those reported previously for the AM260W complex. In the X-ray crystal structure of the AM260W mutant absence of the Q_A ubiquinone was accompanied by repacking of a short loop of amino acids connecting the membrane-spanning E helix and the surface de helix, involving four residues adjacent to the site of mutation at Ala M260 (Asn M259, Phe M258, Gly M257, and Met M256). This involved significant changes in orientation of residues Asn M259 and Phe M258 in particular, with the latter moving across to occupy space normally occupied by the isoprenoid side chain of Q_A. This is apparent from the stereoview of overlaid structures shown in Figure 6. Movement of Asn M259 was accommodated by further movements of the side chains of Tyr H40 and Gln H32 away from the Q_A site, as was accompanied changes in the arrangement of buried water molecules (see below). These changes in structure were not seen in the case of the AM248W RC (Figure 4a), and so it is possible to conclude that the repacking of residues M256−M259 in the AM260W RC did not occur simply in response to the cavity created by the absence of the ubiquinone. It seems more likely that the repacking in the AM260W RC was due to specific changes at the adjacent M260 position following replacement of Ala by Trp. In fact, the CA−CB bond of the Ala M260 residue in the wild-type complex occupies a somewhat different position to that of Trp M260 in the AM260W mutant, due to the conformation of the remainder of the Trp side chain (see inset to Figure 4b). Steric constraints on the packing of the Trp side chain twist the backbone such that the next few amino acids take up different positions to those adopted in the wild-type complex (Figure 6). In the AM248W RC the CA−CB bond of Trp M248 adopted almost exactly the same position as that of the wild-type Ala residue (see inset to Figure 4a), and so there was no new torsional strain on the adjacent backbone.

Cavity Packing Materials. The engineering of a mutation that prevents incorporation of a largely apolar internal cofactor presents a number of potential problems for the assembly of a protein. In the case of the ubiquinone and BPhe cofactors considered in the present report, the formation of the resulting cavity is accompanied by the absence of a number of potentially stabilizing van der Waals interactions, together with the absence of a smaller number of hydrogen bonds which again may be stabilizing. For the BPhe cofactor, it is known from a combination of spectroscopic and crystallographic data that there are no hydrogen bond interactions between the three carbonyl substituent groups of the macrocycle and the surrounding protein. As a result the absence of the BPhe does not create an unsatisfied hydrogen bond donor at the surface of the resulting internal cavity. However, the Trp introduced at the M149 position has a side chain NH that can act as a hydrogen bond donor, and this projects into the cavity. In the data obtained for the AM149W RC the nitrogen of the Trp side chain was 2.9 Å (center to center) from a spherical electron density feature that could be satisfactorily modeled as a water molecule (teal sphere in Figures 2a and 3b). This water was also within hydrogen bond distance of the side chain OH of Thr M277 and (given the normal location of the H_B BPhe) was positioned approximately halfway across the membrane. Although the depth of this water in the membrane phase may seem somewhat surprising, it should be noted that almost all X-ray crystal structures of the *Rb. sphaeroides* RC include a water molecule located approximately halfway across the membrane at the point at which the D helices of the L- and M-polypeptide cross one another, and so there is a precedent for having a water molecule at such a deeply buried position in this particular membrane protein. Other electron density features occupying the central part of the vacated H_B binding pocket were insufficiently distinctive to be assigned in the final model of the AM149W RC.

Turning to the Q_A site, the headgroup of the ubiquinone includes two keto carbonyl groups that can in principle act as hydrogen bond acceptors. Again, a combination of X-ray crystallography and spectroscopy has shown that one of these keto oxygens accepts a very strong hydrogen bond from the ND1 NH of His M219, while the second accepts a weaker hydrogen bond from the backbone NH of Ala M260 (see ref *26* for a discussion of the relevant literature). The failure

of the ubiquinone to be assembled into the structure of the AM260W or AM248W RC therefore removes these hydrogen bond interactions, as well as introducing a new Trp side chain that carries a potential hydrogen-bonding group.

In both quinone-deficient mutants the internal cavity contained a spherical electron density feature interpreted as a chloride ion (see insets in Figure 4). In both structures this chloride was located between the ND nitrogen of His M219 and the NE nitrogen of Trp M252, at distances of 3.3 and 3.8 Å in the AM248W complex and 3.1 and 3.9 Å in the AM260W complex, with very little movement of these residues in either case. The position of chloride was almost identical in the two structures, an overlay of the two structural models showing a center-to-center difference of only 0.8 Å (data not shown). In both complexes the chloride was also in a position to interact with the NE nitrogen of the new Trp residue, despite their different positions and orientations, with center-to-center distances of 3.3 and 3.1 Å in the AM248W and AM260W complexes, respectively. Thus in both cases the electronegative chloride ion was a suitable shape and charge to occupy a cavity formed by the electropositive Trp M252, Trp (M248 or M260), and His M219 side chains. As discussed previously, it is not clear whether this ion was present in the membrane-bound form of the RC or whether it is introduced during purification and crystallization of the complex. In both cases the chloride was buried deep in the protein interior but was visible from the *intra*membrane surface of the complex through the channel that is normally occupied by the isoprenoid side chain of the Q_A ubiquinone. Nevertheless, the binding position of the chloride was isolated from the extramembrane surface of the RC by the surrounding protein, and given this, it seems more likely that it was incorporated during assembly of the RC, rather than following removal of the complex from the membrane, although this remains conjecture at this stage.

The absence of the Q_A ubiquinone in the AM248W and AM260W RCs and repacking of amino acids M256−M259 in the latter were accompanied by changes in the number and location of electron density features corresponding to buried water molecules. In the case of the AM248W RC a single new water was seen adjacent to the chloride ion (teal sphere in Figure 4a), helping to take up space vacated by the quinone headgroup, but there were no other changes in the arrangement of buried water molecules near the Q_A binding pocket. Other fragmented electron density in the remainder of the vacated Q_A binding pocket was insufficiently distinctive to be modeled. In the case of the AM260W RC, one native water molecule was no longer present due to reorientation of the Asn M259 side chain (orange sphere in Figure 6), and electron density corresponding to three new waters was apparent (teal spheres in Figure 6). Two of these density features were located in space created by reorientation of the Asn M259 side chain (in the center view in Figure 6) and the third in the space created by reorientation of the Phe M258 side chain (on the right in Figure 6).

In the wild-type RC the second hydrogen bond donor to the quinone headgroup is the backbone NH of Ala M260. In the AM248W RC the conformation of this group was unaltered, and it appeared to be free from interactions. In contrast, in the AM260W RC the change to the conformation of the backbone atoms and side chains of amino acids Trp M260 to Gly M257 was such that the backbone NH of the M260 residue no longer pointed toward the cavity created by the absence of the quinone. Instead, this group was in hydrogen bond distance of one of the new water molecules occupying the cavity created by reorientation of the side chain of Asn M259. In addition, the repacking of amino acids M257−M260 involved significant changes to the conformation of the backbone C═O groups of Asn M259, Phe M258, and Gly M257, the backbone NH groups of Asn M259 and Phe M258, and the side chains of Asn M258 and Phe M259. Given the current resolution of X-ray crystal structures for the RC, it is often difficult to be precise about the pattern of hydrogen bonds within the protein, as hydrogen atoms are not resolved and it is difficult to be certain about the correct orientation of side chains such as Asn, for example. Nevertheless, it seems likely that the repacking of amino acids M257−M260 involved the breaking of at least two native hydrogen bond interactions and the creation of up to five new interactions. Some of the latter involved the three new buried water molecules described above. The most prominent change was the large movement of the side chain of Asn M259 (backward and to the right in Figure 6), which brought it into hydrogen-bonding distance of the side chain OH of a Tyr (H40) located toward the cytoplasmic end of the membrane-spanning α-helix of the H-polypeptide. This Tyr had moved away from the new position of Asn M259, as did the side chain of Gln H32 (Figure 6).

Protein Rigidity and Cofactor Exchange. In addition to providing insights into photosynthetic energy transduction, the *Rb. sphaeroides* RC has made a major contribution to our understanding of biological electron transfer (e.g., see ref *27*). This is thanks in no small part to the development of biochemical treatments that bring about removal of the normally tightly bound Q_A ubiquinone and its replacement with a range of alternative redox-active molecules (*28*, *29*). In general terms detergent-solubilized RCs are incubated in the presence of LDAO and the quinone site inhibitor *o*-phenanthroline to remove the native quinone, and this material is then incubated in the presence of an excess of the alternative molecule to achieve replacement. This type of protocol facilitates modulation of the driving force for electron-transfer reactions involving the neutral Q_A center as an acceptor or reduced the Q_A center as a donor (e.g., see refs *29*−*31*). Likewise, protocols have been developed for the removal of the BPhes or monomeric BChls and their replacement with bacteriochlorins with altered substituent groups. These involve incubation of the RC at a carefully controlled temperature in the presence of an excess of the replacement bacteriochlorin (*32*, *33*). Scheer and Struck have commented that temperature is a crucial factor in these bacteriochlorin exchange experiments, it being necessary to heat the protein to close to its "melting temperature" in order to induce sufficient structural flexibility for cofactor exchange to occur, but without causing irreversible structural changes or denaturation (*32*).

The precise mechanisms of these cofactor replacement treatments are not known, but an implication of their success is that the transient protein "husk" formed when the native cofactor is released does not undergo significant changes in structure that would prevent binding of the replacement cofactor. The findings also suggest that the fold adopted by the protein local to each of these binding sites is not

dependent on the presence of the cofactor during assembly. The strongly conserved structures of the AM248W and AM149W mutant RCs are consistent with this implication and go a little further, demonstrating that the absence of either cofactor produces no major changes in the structure of the protein environment. Nevertheless, changes in the stability of the RC arise that can be detected and quantified using the type of approach illustrated in Figure 5. For both Q_A-deficient RCs absence of the quinone produced a decrease in the stability of the membrane-embedded RC, for reasons that can be rationalized in general terms but not (yet) in terms of specific molecular interactions. On the destabilizing side, the exclusion of the ubiquinone in either structure removed two protein−cofactor hydrogen bonds and also removed hydrophobic interactions between the encasing protein and the headgroup of Q_A, plus the first 10 carbon atoms or so of the isoprenoid side chain. In compensation the chloride ion in the Q_A pocket introduced new bonding interactions involving His M219 and two Trp side chains, other bonding interactions were satisfied by new buried water molecules, and presumably additional void spaces were filled by the surrounding lipids or additional water molecules. Nevertheless, the net effect of the many structural changes was somewhat destabilizing in both cases.

One point worth noting is that the AM260W RC showed less destabilization than the AM248W complex (Figure 5), despite showing more extensive changes in structure. This may be due to beneficial effects of the repacking of the residues between M256 and M259 and the incorporation of (net) two additional buried water molecules, with associated bonding interactions. As the overlap of the new Trp with the Q_A ubiquinone was also greater in the case of the AM260W RC, the outcome is that more of the space vacated by Q_A was occupied by protein or other crystallographically resolvable packing materials in this RC than in the AM248W complex.

Absence of the much larger H_B cofactor in the AM149W RC also produced a decrease in thermal stability, but in overall terms this decrease was comparable to that seen on exclusion of Q_A in the AM248W complex. As can be seen in Figure 3, despite being sandwiched at the interface between the membrane-spanning helices of the L- and M-polypeptides, the H_B cofactor is partially exposed to the intramembrane phase. As a result the mutation can be viewed as further deepening an interhelical cleft in the protein surface. Presumably, the shell of annular lipids surrounding the RC undergoes adjustments in terms of the type and location of bound lipids to cope with this deepened cleft, such that although extensive nonpolar protein−cofactor interactions are lost, these are replaced by stabilizing protein−lipid interactions. It may therefore be that a mutation of this type that causes the protein to assemble without a surface-exposed cofactor can be accommodated because the wide variety of lipids potentially available in the bacterial membrane constitutes a structurally flexible environment for the protein. Further structural support can be brought about through the inclusion of new molecules or ions as packing material in the internal voids created in response to mutation, as illustrated by the chloride ions and waters included in the structural models of both quinone-deficient RCs and the water located in the depths of the membrane in the structural model of the BPhe-deficient RC.

REFERENCES

1. Berman, H. M., Westbrook, J., Feng, Z., Gilliland, G., Bhat, T. N., Weissig, H., Shindyalov, I. N., and Bourne, P. E. (2000) The Protein Data Bank, *Nucleic Acids Res. 28*, 235−242.
2. Coleman, W. J., and Youvan, D. C. (1990) Spectroscopic analysis of genetically-modified photosynthetic reaction centers, *Annu. Rev. Biophys. Biophys. Chem. 19*, 333−367.
3. Woodbury, N. W., and Allen, J. P. (1995) The pathway, kinetics and thermodynamics of electron transfer in wild type and mutant bacterial reaction centers of purple nonsulfur bacteria, in *Anoxygenic Photosynthetic Bacteria* (Blankenship, R. E., Madigan, M. T., and Bauer C. E., Eds.) pp 527−557, Kluwer Academic Publishers, Dordrecht, The Netherlands.
4. Van Brederode, M. E., and Jones, M. R. (2000) Reaction centres of purple bacteria, in *Enzyme-Catalysed Electron and Radical Transfer* (Scrutton, N. S., and Holzenburg, A., Eds.) pp 621−676, Kluwer Academic/Plenum Publishers, New York.
5. Wakeham, M. C., and Jones, M. R. (2005) Rewiring photosynthesis: engineering wrong-way electron transfer in the purple bacterial reaction centre, *Biochem. Soc. Trans. 33*, 851−857.
6. Okamura, M. Y., Paddock, M. L., Graige, M. S., and Feher, G. (2000) Proton and electron transfer in bacterial reaction centers, *Biochim. Biophys. Acta 1458*, 148−163.
7. Wraight, C. A. (2004) Proton and electron transfer in the acceptor quinone complex of photosynthetic reaction centers from *Rhodobacter sphaeroides*, *Front. Biosci. 9*, 309−337.
8. Fyfe, P. K., Isaacs, N. W., Cogdell, R. J., and Jones, M. R. (2004) Disruption of a specific molecular interaction with a bound lipid affects the thermal stability of the purple bacterial reaction center, *Biochim. Biophys. Acta 1608*, 11−22.
9. Camara-Artigas, A., Magee, C. L., Williams, J. C., and Allen, J. P. (2001) Individual interactions influence the crystalline order for membrane proteins, *Acta Crystallogr. D 57*, 1281−1286.
10. Thielges, M., Uyeda, G., Camara-Artigas, A., Kalman, L., Williams, J. C., and Allen, J. P. (2005) Design of a redox-linked active metal site: Manganese bound to bacterial reaction centers at a site resembling that of photosystem II, *Biochemistry 44*, 7389−7394.
11. Parson, W. W. (1991) Reaction centers, in *Chlorophylls* (Scheer, H., Ed.) pp 1153−1180, CRC Press, Boca Raton, FL.
12. Parson, W. W. (1996) Photosynthetic bacterial reaction centers, in *Protein Electron Transfer* (Bendall, D. S., Ed.) pp 125−160, BIOS Scientific Publishers, Oxford, U.K.
13. Hoff, A. J., and Deisenhofer, J. (1997) Photophysics of photosynthesis: Structure and spectroscopy of reaction centres of purple bacteria, *Phys. Rep.: Rev. Sect. Phys. Lett. 287*, 2−247.
14. McAuley, K. E., Fyfe, P. K., Ridge, J. P., Cogdell, R. J., Isaacs, N. W., and Jones, M. R. (2000) Ubiquinone binding, ubiquinone exclusion, and detailed cofactor conformation in a mutant bacterial reaction center, *Biochemistry 39*, 15032−15043.
15. Ridge, J. P., van Brederode, M. E., Goodwin, M. G., van Grondelle, R., and Jones, M. R. (1999) Mutations that modify or exclude binding of the Q_A ubiquinone and carotenoid in the reaction center from *Rhodobacter sphaeroides*, *Photosynth. Res. 59*, 9−26.
16. Wakeham, M. C., Goodwin, M. G., McKibbin, C., and Jones, M. R. (2003) Photo-accumulation of the $P^+Q_B^-$ radical pair state in purple bacterial reaction centres that lack the Q_A ubiquinone, *FEBS Lett. 540*, 234−240.
17. Wakeham, M. C., Nabedryk, E., Breton, J., and Jones, M. R. (2004) Formation of a semiquinone at the Q_B site by A-branch or B-branch electron transfer in the reaction centre from *Rhodobacter sphaeroides*, *Biochemistry 43*, 4755−4763.
18. Watson, A. J., Fyfe, P. K., Frolov, D., Wakeham, M. C., Nabedryk, E., van Grondelle, R., Breton, J., and Jones, M. R. (2005) Replacement or exclusion of the B-branch bacteriopheophytin in the purple bacterial reaction centre: the H_B cofactor is not required for assembly or core function of the *Rhodobacter sphaeroides* complex, *Biochim. Biophys. Acta 1710*, 34−46.
19. McAuley-Hecht, K. E., Fyfe, P. K., Ridge, J. P., Prince, S. M., Hunter, C. N., Isaacs, N. W., Cogdell, R. J., and Jones, M. R. (1998) Structural studies of wild type and mutant reaction centres from an antenna-deficient strain of *Rhodobacter sphaeroides*: monitoring the optical properties of the complex from cell to crystal, *Biochemistry 37*, 4740−4750.
20. Otwinowski, Z., and Minor, W. (1997) Processing of X-ray diffraction data collected in oscillation mode, *Methods Enzymol. 276*, 307−326.

21. Navaza, J. (1994) *AMoRe*: an automated package for molecular replacement, *Acta Crystallogr. A 50*, 157−163.
22. Murshudov, G. N., Vagin, A. A., and Dodson, E. J. (1997) Refinement of macromolecular structures by the maximum-likelihood method, *Acta Crystallogr. D 53*, 240−255.
23. Paddock, M. L., Chang, C., Xu, Q., Abresch, E. C., Axelrod, H. L., Feher, G., and Okamura, M. Y. (2005) Quinone (Q_B) reduction by B-branch electron transfer in mutant bacterial reaction centers from *Rhodobacter sphaeroides*: Quantum efficiency and X-ray structure, *Biochemistry 44*, 6920−6928.
24. Watson, A. J., Hughes, A. V., Fyfe, P. K., Wakeham, M. C., Holden-Dye, K., Heathcote, P., and Jones, M. R. (2005) On the role of basic residues in adapting the purple bacterial reaction centre-LH1 photosystem for growth at elevated temperatures, *Photosynth. Res. 86*, 81−100.
25. Hughes, A. V., Rees, P., Heathcote, P., and Jones, M. R. (2006) Kinetic analysis of the thermal stability of the photosynthetic reaction centre from *Rhodobacter sphaeroides*, *Biophys. J. 90*, 4155−4166.
26. Breton, J., Lavergne, J., Wakeham, M. C., Nabedryk, E., and Jones, M. R. (2007) The unusually strong hydrogen bond between the carbonyl of Q_A and His M219 in the *Rhodobacter sphaeroides* reaction center is not essential for efficient electron transfer from Q_A^- to Q_B, *Biochemistry 46*, 6468−6476.
27. Moser, C. C., Keske, J. M., Warncke, K., Farid, R. S., and Dutton, P. L. (1992) Nature of biological electron transfer, *Nature 355*, 796−802.
28. Okamura, M. Y., Isaacson, R. A., and Feher, G. (1975) Primary acceptor in bacterial photosynthesis—obligatory role of ubiquinone in photoactive reaction centers of *Rhodopseudomonas spheroides*, *Proc. Natl. Acad. Sci. U.S.A. 72*, 3491−3495.
29. Gunner, M. R., Robertson, D. E., and Dutton, P. L.(1986) Kinetic-studies on the reaction center protein from R*hodopseudomonas sphaeroides*—the temperature and free-energy dependence of electron-transfer between various quinones in the Q_A site and the oxidized bacteriochlorophyll dimer, *J. Phys. Chem. 90*, 3783−3795.
30. Woodbury, N. W., Parson, W. W., Gunner, M. R., Prince, R. C., and Dutton, P. L. (1986) Radical-pair energetics and decay mechanisms in reaction centers containing anthraquinones, naphthoquinones or benzoquinones in place of ubiquinone, *Biochim. Biophys. Acta 851*, 6−22.
31. Warncke, K., and Dutton, P. L. (1993) Influence of Q_A site redox cofactor structure on equilibrium binding, in situ electrochemistry, and electron-transfer performance in the photosynthetic reaction center protein, *Biochemistry 32*, 4769−4779.
32. Scheer, H., and Struck, A. (1993) Bacterial reaction centers with modified tetrapyrrole chromophores, in *The Photosynthetic Reaction Center* (Deisenhofer, J., and Norris, J. R., Eds.) Vol. 1, pp 157−192, Academic Press, San Diego, CA.
33. Scheer, H., and Hartwich, G. (1995) Bacterial reaction centers with modified tetrapyrrole chromophores, in *Anoxygenic Photosynthetic Bacteria* (Blankenship, R. E., Madigan, M. T., and Bauer, C., Eds.) pp 649−663, Kluwer Academic Publishers, Dordrecht, The Netherlands.
34. Cruickshank, D. W. J. (1999) Remarks about protein structure precision, *Acta Crystallogr. D 55*, 583−601.

BI701085W